Ab initio investigations of the Ca$_2$IrO$_4$-type structure as a "post-K$_2$NiF$_4$": Case study of Na$_2$OsO$_4$

Samir F. Matar [a,*], Gérard Demazeau [a], Naïm Ouaini [b]

[a] CNRS, University of Bordeaux, ICMCB, 87 avenue du Docteur Albert Schweitzer, 33600 Pessac, France
[b] Université Saint Esprit de Kaslik, USEK, Faculté des Sciences, URA GREVE (CNRS/USEK/UL), Jounieh, Lebanon

ARTICLE INFO

ABSTRACT

Deriving the energy–volume equation of state for Na$_2$OsO$_4$ in its actual Ca$_2$IrO$_4$-type structure at high pressure and in hypothetic K$_2$NiF$_4$-type, leads to energy destabilization at a larger volume for the latter and to propose the former as a post-K$_2$NiF$_4$ through which a tuning of the magnetism and conductivity can be achieved: while the oxide system is magnetically silent in Ca$_2$IrO$_4$-type due to spin pairing ($S = 0$ for d^2 Os^{6+}) with a semi-conducting behavior, a finite moment develops in the latter when spin polarization is accounted for ($S = 1$).

1. Introduction

The discovery of the high pressure structural transformation of perovskite (PV) to the post-perovskite (PPV) with CaIrO$_3$-type structure [1–4], inspired by geosciences, led to a novel approach in materials chemistry as the synthesis of denser materials due to the passage from corner sharing octahedra in PV to edge sharing octahedra in PPV together with a reduced dimensionality: 3D (PV) → 2D-like (PPV).

On the other hand, the structural type Ca$_2$IrO$_4$ [5,6], has a quasi-1D structure formed of chains of edge sharing IrO_6 octahedra along the c-axis as sketched in Fig. 1a. One reduced dimensionality A$_2$BO$_4$-type structure is the tetragonal K$_2$NiF$_4$-type (KNF) which has corner sharing octahedra in a succession of perovskite (ABO$_3$) and rock salt (AO) layers (Fig. 1b). Consequently, in parallel of the 3D (PV) → 2D (PPV) transformation with pressure, it is proposed here that 2D KNF could be considered, as a low pressure analog of 1D-Ca$_2$IrO$_4$ PKNF. Such a new concept is able to open perspectives of syntheses of novel materials. In this work we argue on this, based on energy criteria derived *ab initio* from the energy–volume equation of state and an examination of the electronic band structure.

Until recently the only member of the Ca$_2$IrO$_4$-type structure was the archetype itself [5,6]. But recently Shi et al. [7] have identified this structure for Na$_2$OsO$_4$, synthesized under high pressures. Despite the d^2 configuration of namely hexavalent osmium, Os^{6+}, the system was found from experiment and calculations [7] as magnetically non active ($S = 0$; spin pairing) while one would expect $S = 1$ for two – unpaired – spins in t$_{2g}$ manifold. An explanation was proposed on the basis of a strong distortion of the OsO_6 octahedron whereby the degeneracy of the t$_{2g}$ orbitals is lifted resulting in pairing of the two spins. We show through this scheme that the physical properties can be tuned such as the metal insulator transition and the onset of a magnetic moment on Os in Na$_2$OsO$_4$ illustrated here.

2. Computational methodology

The calculations are conducted within the well established quantum theoretical framework of density functional DFT [8,9]. Within DFT, a pseudo-potential approach within the VASP code [10] is used first to geometry-optimize atomic positions and lattice parameters. Then the equation of state (EOS) is obtained through energy–volume curves fitted with a Birch EOS [11]. For these purposes, we call for the accurate projector augmented wave (PAW) method [12,13] within the generalized gradient approximation (GGA) following the scheme of Perdew, Burke and Ernzerhoff for

* Corresponding author.
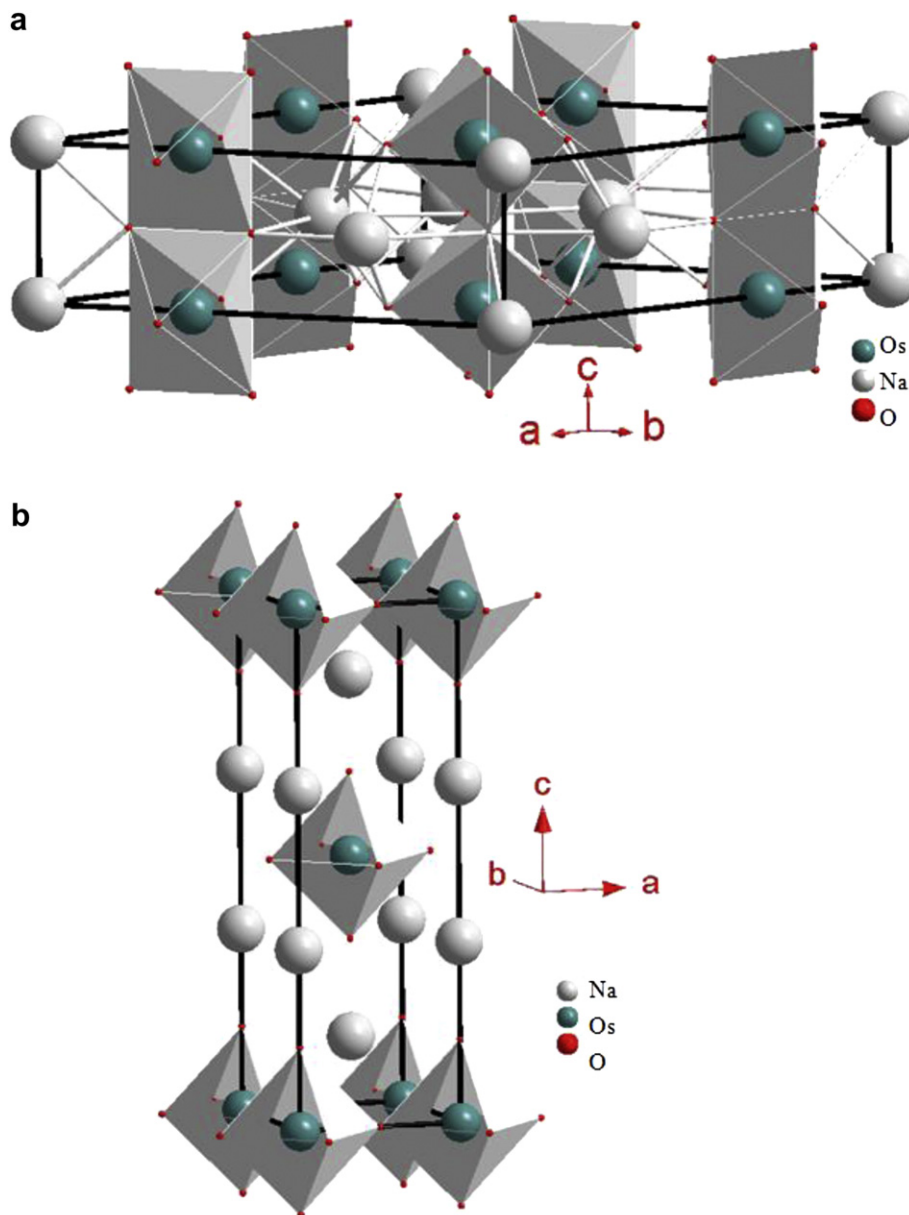E-mail address: matar@icmcb-bordeaux.cnrs.fr (S.F. Matar).

a

b

Fig. 1. Na$_2$OsO$_4$ structure in (a) high pressure experimental structure with chains of edge sharing OsO_6 octahedra parallel to the c axis; (b) hypothetic K$_2$NiF$_4$ structure.

the treatment of exchange and correlation effects [14]. The calculations are converged at an energy cut-off of 400 eV. The k-point integration is carried out with a starting mesh of $4 \times 4 \times 4$ up to $8 \times 8 \times 8$ for best convergence and relaxation to zero strains [15]. The Brillouin-zone integrals are approximated using a special k-point sampling following Blöchl [13].

For a full description of the electronic band structures and of chemical bonding, the scalar relativistic all-electrons augmented spherical wave (ASW) [16] method is used. Like in the calculations with pseudo-potentials, the exchange and correlation effects are accounted for within the GGA functional [14]. In the ASW method, the wave function is expanded in atom-centered augmented spherical waves, which are Hankel functions and numerical solutions of Schrödinger's equation, respectively, outside and inside the so-called augmentation spheres. In order to optimize the basis set, additional augmented spherical waves are placed at carefully selected interstitial sites (IS). The choice of these sites as well as the augmentation radii are automatically determined using the sphere-

geometry optimization algorithm [17]. Self-consistency is achieved by a highly efficient algorithm for convergence acceleration [18]. The Brillouin-zone integrations are performed using the linear tetrahedron method [13]. In the minimal ASW basis set, we have chosen the outermost shells to represent the valence states using partial waves up to $l_{max.} + 1 = 3$ for Os and $l_{max.} + 1 = 2$ for Ca, O and IS. Low energy lying O (2s) are considered as core states. The completeness of the valence basis set is checked for charge convergence. The self-consistent field calculations are run to a convergence of $\Delta Q = 10^{-8}$ for the charge density and the accuracy of the method is in the range of about 10^{-8} Ryd. (1 Ryd. = 13.6 eV) regarding energy differences.

The relative magnitude of the chemical bonding is obtained based on the overlap population analysis: S_{ij}, i and j being two chemical species. The crystal orbital overlap population (COOP) [19] criterion is used. In the plots positive, negative and zero COOP magnitudes indicate bonding, anti-bonding and non-bonding interactions respectively.

3. Geometry optimization and equation of state

Starting from the lattice parameters and the internal atom coordinates of Na_2OsO_4 [7] and of the known K_2NiF_4 structural type, we carried out a full geometry optimization. The results in Table 1 show small deviation with respect to the experimental data [7] for the atomic positions and the Os–O distances as well as a smaller magnitude of the volume; this could be due to the choice of the potentials. Let us mention here that the calculated total energy pertains to the cohesive energy within the crystal. In as far as the zero of energy depends on the choice of the pseudo-potentials, somehow it becomes arbitrary; i.e. it is shifted but not scaled. However the energy derivatives – as well as the EOS – remain unaltered. For this reason one needs to establish the EOS and extract the fit parameters for an assessment of the equilibrium values. This is done from an (E, V) set of calculations around the minima found from geometry optimization. The resulting $E = f(V)$ curves given in Fig. 2 have a quadratic variation which can be fitted with energy–volume Birch EOS to the 3rd order [11]:

$$E(V) = E_o(V_o) + [9/8]V_oB_o\left[\left([(V_o)/V]\right)^{[2/3]}-1\right]^2 \\ + [9/16]B_o(B'-4)V_o\left[\left([(V_o)/V]\right)^{[2/3]}-1\right]^3,$$

where E_o, V_o, B_o and B' are the equilibrium energy, the volume, the bulk modulus and its pressure derivative, respectively. The fit results are given in the insert of Fig. 2. For sake of comparison the values are given for three formula units (fu) in both structures, i.e. with 3 times the equilibrium values of energy and volume for the compound in the K_2NiF_4 structure. For the experimental Ca_2IrO_4-type structure, there is a good agreement for the cell volume: 252.6 Å^3 versus the calculated equilibrium value $V_0 = 246.7$ Å^3. Note that the latter value is closer to experiment than the geometry optimized value for the reasons stated above leading to establish the respective EOS.

The experimental structure (PKNF) is found at lower energy, stabilized by 1.44 eV versus KNF and the zero pressure bulk modulus B_0 is slightly larger than with KNF. However both values are smaller than the range of the oxides for which B_0 amounts to $\sim$200 GPa such as the (PV) and (PPV) $CaRhO_3$ – Ref. [4] and therein cited works –. This is likely due to the lower dimensionality of the structures under consideration. Despite the stabilization of the PKNF structure in the volume range below 270 Å^3, the crossing of the two curves at 280 Å^3, is noteworthy in as far as the K_2NiF_4-type would become stabilized at larger volumes. In both varieties, the magnitude of B' amounts to $\sim$4, a value usually encountered [4].

Table 1
Na_2OsO_4: Crystal characteristics with Wyckoff positions in respective space groups for hypothetic K_2NiF_4-type and true Ca_2IrO_4-type.

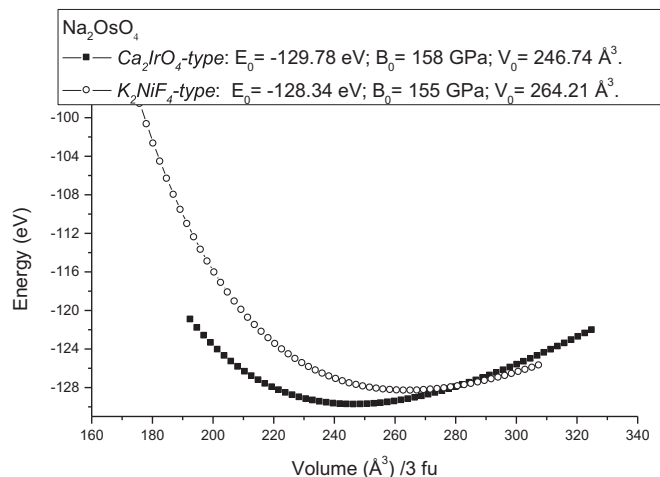| Na_2OsO_4	K_2NiF_4-type (hypo.)	Ca_2IrO_4-type (this work)	Ca_2IrO_4-type [Shi 7]
Space group	$I4/mmm$ $Z = 1$	$P\ 6\ m2$; $Z = 3$	
Na1	0, 0, 0.346 at K (4e)	0,0,0	0,0,0 (1a)
Na2		⅓ , ⅔ , ½	⅓ , ⅔ , ½ (2d)
Na3		0.699, 0, ½	0.6943, 0, ½ (3g)
Os	0,0,0 at Ni (2a)	0.330, 0, 0	0.3296, 0, 0 (3f)
O1	0,0,0.16 at F1 (4e)	0.190, 0, ½	0.1935, 0, ½ (3g)
O2		0.461, 0, ½	0.4580, 0, ½ (3g)
O3	0, ½, 0 at F2 (4c)	0.437, 0.224, 0	0.4308, 0.2127, 0 (6j)
a (Å)	3.81	9.32	9.61
c/a	2.97	0.34	0.33
Volume (Å^3)	86.2	238.1	252.6
d (Os–O) Å	1.89 (O1)	2.05 (O1)	2.05 (O1)
	1.91 (O2)	2.00 (O2)	2.00 (O2)
		1.81 (O3)	1.77 (O3)

Fig. 2. Energy–volume equation of state for the two varieties of Na_2OsO_4 with equilibrium values from Birch EOS in the insert.

4. Electronic structure and chemical bonding

Using the calculated lattice positions for K_2NiF_4 (Table 1) and the experimental values to enable comparisons, we calculate the electronic structures and the properties of chemical bonding for with ASW method both varieties. At self-consistent convergence, charge transfer is observed from Na and Os toward O and IS with amounts of $\sim$0.5–1 electron. These transfers are not meaningful of an ionic character such as O^{2-}, not encountered in such calculations on one hand and they point to a covalently bonded oxide on the other hand.

4.1. Ca_2IrO_4-type Na_2OsO_4

The site projected density of states (DOS) for a spin degenerate configuration (NSP, non spin polarized) is shown in Fig. 3a. They exhibit similarities with the results of Shi et al. [7] such as for the small energy gap at the top of the valence band (VB) – energy reference in this plot and following ones – between the Os d states. Also LDA + U subsidiary calculations, meant to enhance electron correlations in an oxide compound, did not allow larger opening of the gap. Due to their s character the Na states are smeared over the whole energy range of VB and conduction band (CB). The similar DOS shapes of oxygen with osmium signals the chemical bonding with two main regions: {−8, −4 eV} and {−4, 0 eV}. This is illustrated by the COOP plots in Fig. 3b with, respectively, intense σ-like bonding and less intense bonding which is π-like. Antibonding counter parts are observed within the CB. Also O3 partial DOS are found most intense due to their twice larger multiplicity versus O1 and O2 but they show less hybridized character in the {−4 eV, 0} energy region. This suggests their implication with σ-like bonding only and no COOP between −5 and 0 eV, contrary to O1 and O2 which are involved with both σ- and π-like bonding. Considering the OsO_6 octahedron, such a feature could be expected in as far as O1 and O2 with d (Os-O1/O2 $\sim$2 Å) are equatorial while O3 which has the shortest distance to Os ($\sim$1.8 Å) is apical.

4.2. K_2NiF_4-type Na_2OsO_4

Contrary to the true type structure, the site projected density of states (DOS) for a spin degenerate configuration (NSP, non spin polarized) in Fig. 4a exhibits the characteristics of large density of states at the Fermi level (E_F) due to Os d states. Note that the
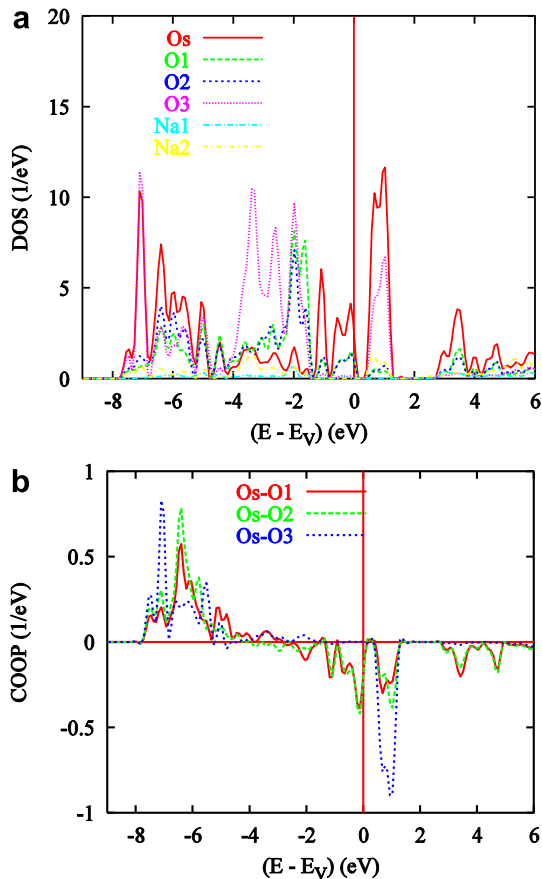
Fig. 3. Na_2OsO_4 true type. (a) Site projected density of states; (b) chemical bonding with COOP criterion.

belonging of Os to the 3rd transition metal period should characterize a broad d band which does not normally (in alloys, electron gas correlations) sustain enough localization for the development of on-site magnetic moment. However in an oxide compound the electron correlations are larger and the d states are more localized, i.e. they develop larger density of states at the Fermi level. In the Stoner mean field theory of band ferromagnetism [20] this signals instability of the NSP configuration and the system minimizes its energy when spin polarization (SP) is allowed. This is also observed for the O1 partial DOS (PDOS) at E_F albeit with a smaller intensity. As in the above section, the lower part of the VB, below -4 eV, is engaged with σ-like Os–O bonding with prevailing O2 between -7 and -9 eV, then O1 states are more involved from -4 eV up to E_F, either with π-like bonding or with a non-bonding character. The results can be further assessed in a chemical bonding qualitative analysis.

Fig. 4b shows the different 1:1 interactions. The Na–O bonding is of low magnitude due to the non-directional s-like character of the Na orbitals involved. On the contrary differences can be observed of Os–O bonding where O p orbitals are involved; it is found larger for O2 than for O1. The respective distances close to 1.9 Å cannot be at the origin of these differences; it is rather due to the prevailing σ-like bonding for O2 and the π-like one for O1. Both Os-O1 and Os-O2 show anti-bonding peaks at E_F but the former are dominant, concomitantly with the presence of large O1 DOS at E_F.

In view of the large DOS at E_F signaling a magnetic instability, subsequent spin polarized calculations are then carried out by allowing electrons to be distributed over two spin channels: ↑ and ↓. Note that we are just checking out the tendency of Os (and possibly O1) to develop an on-site magnetic moment, not the long
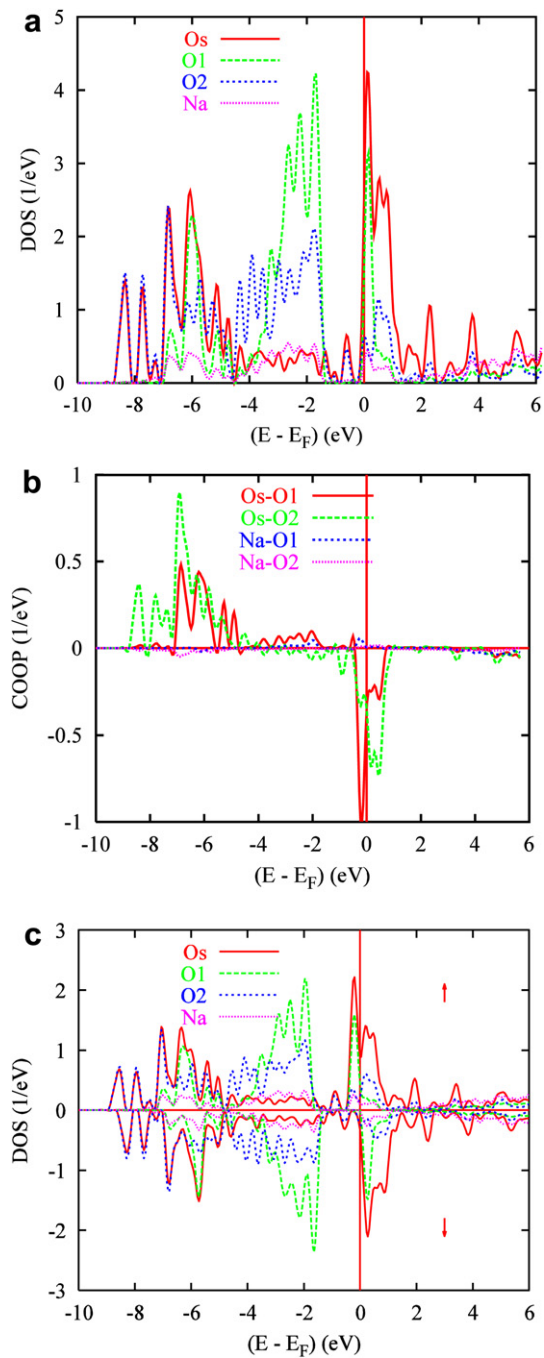

Fig. 4. Na_2OsO_4 in K_2NiF_4-type. (a) NSP Site projected density of states; (b) NSP chemical bonding and (c) Magnetic calculations (SP): Site and spin projected density of states.

range magnetic order which could be ferro- or anti-ferromagnetic; the latter being most common in oxides. The magnetic solution leads to an energy stabilization of $\Delta(E_{SP}-E_{NSP}) = -0.06$ eV/fu and the development of a magnetic moment on Os and O1 of respectively 0.71 μ_B and 0.23 μ_B (with a total magnetic moment of 0.94 μ_B, close to 1) while O2 has a residual moment of -0.02 μ_B of induced nature due to the bonding with the metal. This is illustrated by the SP-DOS in Fig. 4c which are descriptive of a half-metallic ferromagnet because of the crossing of E_F at a large magnitude for majority spin DOS (↑) while vanishingly small DOS are observed for minority spin (↓).

The consequence is that in the KNF structure the system is magnetically active and behaves as a metal − at least in the considered magnetic configuration − while in the PKNF form it is semi-conducting and magnetically silent. This is due to spin pairing [7] in the split t_{2g} manifold in a highly distorted OsO_6 octahedron. On the contrary, despite the D_{4h} point symmetry of OsO_6, with close Os-O1 and Os-O2 distances of ~1.9 Å, the splitting of the octahedron does not lead to spin pairing and the $S = 1$ state is the ground state which is then magnetically active.

We propose that the PKNF form could be stabilized through a preparation method improving the kinetics such as a solvothermal process using moderated oxidizing pressures able to stabilize osmium (VI) but in presence of a specific solvent able to promote the kinetics [21]. Such investigations are underway.

5. Conclusion

The high pressure transformation of perovskite with corner sharing octahedra to the post-perovskite with edge sharing octahedra involves a densification and a reduced dimensionality from 3D to 2D-like. In parallel, we propose: based on energy criteria derived within DFT, the reduced dimensionality (1D) Ca_2IrO_4 structure as a potential post-K_2NiF_4. This is illustrated here with recently evidenced Na_2OsO_4. Using DFT based methodology, the energy−volume equation of state of Na_2OsO_4 in its actual structure (Ca_2IrO_4-type) leads to an equilibrium volume in agreement with experiment. In a K_2NiF_4 hypothetic structure the volume is 7% larger with an energy destabilization. While the oxide is magnetically silent due to spin pairing ($S = 0$ for d^2 Os^{6+}) with a semi-conducting behavior, a finite moment in a closely half-metallic ferromagnet develops in the latter when spin polarization is accounted for ($S = 1$). This lets suggest the occurrence of the Ca_2IrO_4-type structure as a post-K_2NiF_4 and a tuning of the magnetism and conductivity through this scheme.

References

[1] G. Fiquet, Z. Krist 216 (2001) 248.
[2] A.R. Oganov, S. Ono, Nature 430 (2004) 445.
[3] M. Murakami, K. Hirose, K. Kawamura, N. Sata, Y. Ohishi, Science 304 (2004) 855.
[4] S.F. Matar, G. Demazeau, A. Largeteau, Solid State Sci. 12 (2010) 373.
[5] H.K. Müller-Buschbaum, J. Alloys Comp 349 (2003) 49.
[6] D. Babel, W. Rüdorff, R. Tschöpp, Z. Anorg. Allg. Chem. 347 (1966) 282.
[7] Y.G. Shi, Y.F. Guo, S. Yub, M. Arai, A.A. Belik, A. Sato, K. Yamaura, E. Takayama-Muromachi, T. Varga, J.F. Mitchel, J. Solid State Chem. l83 (2010) 402.
[8] P. Hohenberg, W. Kohn, Phys. Rev. 136 (1964) B 864.
[9] W. Kohn, L.J. Sham, Phys. Rev. 140 (1965) A 1133.
[10] G. Kresse, J. Furthmüller, Phys. Rev. B. 54 (1996) 11169.
[11] F. Birch, J. Geophys. Res 83 (1978) 1257.
[12] G. Kresse, J. Joubert, Phys. Rev. B. 59 (1999) 1758.
[13] P.E. Blöchl, Phys. Rev. B. 50 (1994) 17953.
[14] J. Perdew, K. Burke, M. Ernzerhoff, Phys. Rev. Lett. 77 (1996) 3865.
[15] H.J. Monkhorst, J.D. Pack, Phys. Rev. B. 13 (1976) 5188.
[16] A.R. Williams, J. Kübler, C.D. Gelatt, Phys. Rev. B. 19 (1979) 6094.
[17] V. Eyert, K.H. Höck, Phys. Rev. B. 57 (1998) 12727.
[18] V. Eyert, J. Comput, Phys 124 (1996) 271.
[19] R. Hoffmann, Angew. Chem. Int. Ed. Engl. 26 (1987) 846.
[20] P. Mohn, Magnetism in the Solid State − An Introduction, Springer Series In: Solid-State Sciences. Springer, Heidelberg, 2003.
[21] G. Demazeau, Z. Naturforsch 65b (2010) 999.